Frontiers of Physics
https://doi.org/10.1007/s11467-018-0874-z
Front. Phys.
14(2), 23605 (2019)

RESEARCH ARTICLE

Linear dipole behavior of single quantum dots encased in metal oxide semiconductor nanoparticles films

Guo-Feng Zhang[1,4,†], Yong-Gang Peng[2], Hai-Qing Xie[3], Bin Li[1], Zhi-Jie Li[1], Chang-Gang Yang[1], Wen-Li Guo[1], Cheng-Bing Qin[1,4], Rui-Yun Chen[1,4], Yan Gao[1,4], Yu-Jun Zheng[2], Lian-Tuan Xiao[1,4,‡], Suo-Tang Jia[1,4]

[1] *State Key Laboratory of Quantum Optics and Quantum Optics Devices, Institute of Laser Spectroscopy, Shanxi University, Taiyuan 030006, China*
[2] *School of Physics, Shandong University, Jinan 250100, China*
[3] *Department of Physics, Taiyuan Normal University, Jinzhong 030619, China*
[4] *Collaborative Innovation Center of Extreme Optics, Shanxi University, Taiyuan 030006, China*
Corresponding authors. E-mail: [†] *guofeng.zhang@sxu.edu.cn,* [‡] *xlt@sxu.edu.cn*
Received September 11, 2018; accepted November 10, 2018

Understanding of charge/energy exchange processes and interfacial interactions that occur between quantum dots (QDs) and the metal oxides is of critical importance to these QD-based optoelectronic devices. This work reports on linear dipole behavior of single near-infrared emitting CdSeTe/ZnS core/shell QDs which are encased in indium tin oxide (ITO) semiconductor nanoparticles films. A strong polarization anisotropy in photoluminescence emission is observed by defocused wide-field imaging and polarization measurement techniques, and the average polarization degree is up to 0.45. A possible mechanism for the observation is presented in which the electrons, locating at single QD surface from ITO by electron transfer due to the equilibration of the Fermi levels, result in a significant Stark distortion of the QD electron/hole wavefunctions. The Stark distortion results in the linear polarization property of the single QDs. The investigation of linear dipole behavior for single QDs encased in ITO films would be helpful for further improving QD-based device performance.

Keywords single quantum dots, linear dipole behavior, electron transfer, polarization property, metal oxide nanoparticles

1 Introduction

Quantum dot (QD)-metal oxide semiconductor nanoparticle junctions are an integral part of next-generation solar cells, light emitting diodes, and nanostructured electronic arrays [1–4]. Understanding of charge/energy exchange processes and interfacial interactions that occur between quantum dots (QDs) and the metal oxides is of critical importance to these QD-based photovoltaic and optoelectronic devices [5–9]. The metal oxides are generally used as the electron and hole acceptors, and excitons in QDs can be dissociated by transferring the electrons and holes to the metal oxide [10]. When QDs are coupled with large bandgap metal oxide semiconductors such as TiO_2, ZnO, SnO_2 and indium tin oxide (ITO), where match of energy levels, charge injection efficiency, and interface dielectric effect are always needed to be carefully considered. In the QD-based photovoltaic devices, such as QD-based Schottky junction solar cell [11, 12] and p-n homojunction solar cell [13, 14], ITO as transparent electrode directly contacts with QD layer. Especially the p-n homojunction QD solar cell represents the most recent development, which has been used to further address the limitations of low open-circuit voltage and stability. This type of QD solar cell is believed to hold high promise and open the avenue to prospective inverted p-n homojunction and multijunction photovoltaic devices.

Recently, key insights into mechanisms and time scales for charge and energy transport between QDs and ITO nanoparticles have been provided by time-resolved photoluminescence (PL) studies [5, 15–22]. Interfacial charge transfer from ITO to QDs and formation of negatively charged QDs can suppress blinking dynamics of single QDs and reduce the PL lifetimes [5, 20], and the spectral peak emission energies show a red shift as large as approximately −35 meV with respect to that of single QDs on glass substrates [17]. The ITO also introduces an extra nonradiative energy transfer to reduce PL intensity of QDs [22] and modify photon emission statistics of single QDs [19, 21].

Generally, the band-edge exciton transitions in single

QDs are unpolarized in absorption and emission [23–27], unlike the strictly linearly polarized transitions in conjugated organic molecules described in the literatures [28–32]. Detailed theoretical models of CdSe QDs predict a manifold of transitions, and the emission originates from two degenerate states with orthogonal dipole orientations [33, 34]. The studies about deviations from the degenerate behavior so far have been mainly focused to asymmetric QDs [35–39]. Enforcing directionality in the transition moment of individual QDs is very difficult. However, the linearly polarized absorption and emission have been found in individual CdSe QDs surface-functionalized with monodisperse oligo-phenylene vinylene (OPV) ligands, which was attributed to the QD surface electrons from the photoexcited ligands inducing a significant Stark distortion of the QD electron/hole wavefunction [40]. The observations have been supported by perturbation calculations of the Stark-induced wavefunction distortion and induced linear polarization [41]. In addition, the enhanced spectral stability, suppressed fluorescence blinking, polarization-induced spectral shifts and multiexcitonic emission have also been observed in the CdSe/OPV system [41–43], which are quite similar with the observations in QD/ITO systems mentioned above. The electrons at single QD surface could profoundly affect QD luminescence properties. However, the polarization property of single QDs encased in ITO films linking excess surface electrons has not been investigated yet.

Here, we investigate the linearly polarized emission of single near-infrared (NIR) emitting CdSeTe/ZnS_{3ML} core/multishell QDs encased in ITO films. The linearly polarized emission of single QDs is observed by defocused wide-field fluorescence imaging microscopy, and the polarization degree is measured by single particle polarization microscopy. We attribute the linear dipole behavior to the surface electrons inducing the Stark distortion of the QD electron/hole wavefunctions. The investigation of linear dipole behavior for single QDs encased in the ITO films would be helpful for further improving photovoltaic device performance.

2 Experimental section

2.1 Preparation of single QDs/ITO nanostructure sample

Schematic view of the sample preparation is depicted in Fig. 1(a). The NIR emitting CdSeTe/ZnS_{3ML} core/multishell QDs (Qdot®800ITKTM Organic QDs) were ordered from Thermo Fisher Scientific Inc. The transmission electron microscope (TEM) image of single QDs is shown in Fig. 1(b). The size of the QDs is 8.3±2.1 nm and the diameter of core is ∼ 6.4 nm. Absorption and emission spectra are shown in Fig. 1(c), and the maximum PL emission wavelength is ∼ 800 nm. The QDs with a band gap of ∼ 1.5 eV were selected, since the 1.5 eV is the optimum band gap for maximum power conversion in solar cells [44]. The ITO nanoparticles (< 100 nm particle size (DLS), 30 wt. % in isopropanol, Sigma-Aldrich) were centrifuged at 3000 rpm for 5 minutes, then we wiped out the supernatant, and the precipitate was dispersed in toluene with a

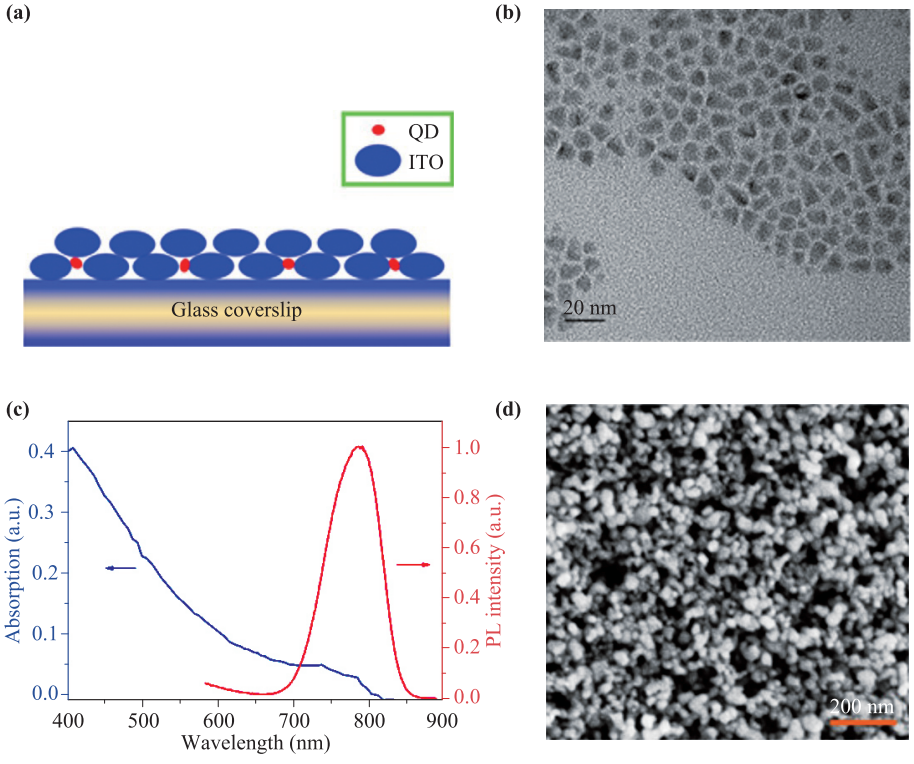

Fig. 1 Schematic view of sample preparation and material characteristics. **(a)** The schematic of single quantum dots (QDs) encased in indium tin oxide (ITO) nanoparticles films. **(b)** Transmission electron microscope (TEM) image of single near-infrared emitting CdSeTe/ZnS_{3ML} core/multishell QDs. **(c)** Absorption and emission spectra of CdSeTe/ZnS_{3ML} core/multishell QDs in solution. **(d)** Scanning electron microscope (SEM) image of the ITO nanoparticles spin-coated onto glass coverslip.

concentration of ∼ 15 wt.%. At last, single QDs solution (10^{-8} mol·L^{-1}) in toluene was added to the dispersion and formed a mixture with single QDs (∼ 10^{-9} mol·L^{-1}). The mixture was spin-coated onto a cleaned glass coverslip with a rotational speed of 3000 rpm to form an ITO nanoparticles film encasing single QDs. ITO film with the thicknesses of ∼ 350 nm was obtained. The samples were placed in vacuum at 315 K for 3 hours to remove the residual solvent. Figure 1(d) presents a scanning electron microscope (SEM) image of spin-coated ITO nanoparticles onto glass coverslip.

2.2 Defocused wide-field fluorescence microscopy

The defocused wide-field fluorescence imaging was performed using an inverted optical microscope (IX71, Olympus) equipped with an oil immersion objective (Plan Fluorite, Olympus, 100×, 1.3 NA) and an EMCCD camera (ProEM: 512B, Princeton Instruments). The 635 nm light from a diode-pumped solid-state laser (MLL-III-635L, Changchun) was used as the excitation source. The excitation light was passed through a $\lambda/2$ and a $\lambda/4$ waveplate to form a circular polarization light. PL was collected by the same objective and passed through a dichroic mirror and a long pass filter (z635rdc and HQ655LP, Chroma Technology Co.). The image was further magnified 3.3 times with an additional lens (the resulting maximum view of image is 24.6 μm × 24.6 μm). The excitation field contains only a limited contribution of radial or z-polarized light when using a standard Köhler illumination and therefore the excitation of molecules oriented along z-axis is disfavored. To overcome this problem a quasi-total internal reflection mode (qTIRF) has been employed [45]. Using qTIRF, the intensity of the z-component of the excitation was increased. And the angular resolution on both of radial and azimuthal orientation can be drastically increased [45]. In order to perform real 3D imaging, the wide field system has been modified by working slightly out of focus to perform so called defocused wide field imaging. Typically, the objective was transferred toward sample by 0.8–1.2 μm from focused position. Sequences of defocused images up to 2000 frames have been recorded with an integration time of 100 ms. The resulting defocused images were analyzed with a home-built MatLab routine according to the theoretical model [46, 47].

2.3 Single particle polarization microscopy

The experimental setup for the single QDs fluorescence microscope has been shown previously [20, 30]. A picosecond pulsed diode laser (PDL800-D PicoQuant, $\lambda = 635$ nm) was used to excite single QDs. The output of the pulse laser was passed through a $\lambda/2$ and a $\lambda/4$ waveplate to change the polarized laser into circular polarization light. The beam was sent into a conventional inverted fluorescence microscope (IX71, Olympus Plan Fluorite, Olympus) from its back side, reflected by a dichroic mirror (Z635RDC, Chroma Technology Co.), and focused by an oil immersion objective lens (Olympus, 100×, 1.3 NA) onto the upper sample surface of the glass coverslip. The PL was collected by the same objective lens and then passed through the dichroic mirror, an emission filter (HQ655LP, Chroma Technology Co.), and a notch filter (BrightLine, Semrock, NF03-633E-25), was focused onto a 100 μm pinhole for spatial filtering to reject out-of-focus photons. PL photons were subsequently sent to a rotating achromatic half-wave plate (AHWP10M-980, 690–1200 nm) combined with a broadband polarizing beamsplitter cubes (Thorlabs, PBS122) to measure the polarization degree. The polarization beam splitter divides the PL photons into its two components which are subsequently focused through two lenses and collected by two single photon detectors (PerkinElmer, SPCM-AQR-15). The two detectors are used to detect horizontal and vertical polarization photons, respectively. A piezo-scan stage (Piezosystem jena, Tritor 200/20 SG) with an active x-y-z feedback loop mounted on the inversion microscope was used, and the sample was scanned over the focus of the excitation spot, producing a two-dimensional fluorescence imaging. The signals from the single photon detectors are recorded by a time-correlation single photon counting (TCSPC) data acquisition card (HydraHarp 400, PicoQuant) to obtain PL information of single QDs. For reducing the effects of the QD charged states on the polarization degree [48], we chose a low-power excitation condition: the pump fluence of laser is set at the average number of photons $\langle n \rangle =\sim 0.30$ absorbed per QD per pulse [21, 49]. All measurements were performed at room temperature.

3 Results and discussion

3.1 Defocused imaging of single QDs

In the first section, we employ the defocused wide-field imaging method to investigate linear dipole behavior of single QDs encased in ITO films. Since the defocused imaging technique is based on the electron transition dipole approximation and the fact that the dipole radiation exhibits an angular anisotropy, the anisotropy in the defocused imaging provides information on the transition dipole axis. The dipole system of QD is assumed to be a superposition of an elliptic dipole plus a perpendicular dipole or of three perpendicular linear dipole with different emission intensity [50]. Here we use the model of three perpendicular dipoles as sketched in Fig. 2(a). As shown, (x, y, z) and (X, Y, Z) indicate dipole system and the coordinates of lab system, respectively. The orientation of this dipole system with respect to the lab system can be defined by three Euler angles Ω, Ψ, and ω. The Z axis is the optical axis. The defocused wide-field fluorescence

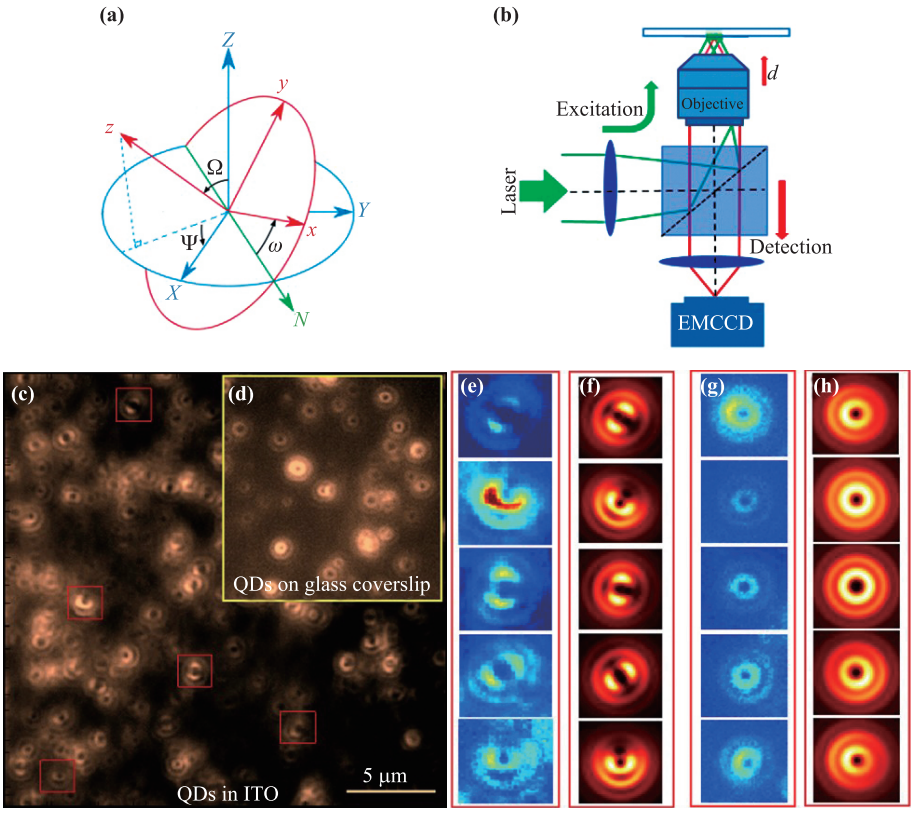

Fig. 2 Schematic of three-dimensional (3D) orientation of quantum dot (QD) and experimental setup, and defocused images of single QDs encased in ITO film and on glass coverslip. **(a)** Sketch of the simulation model to define the emission from a QD. The 3D orientation of the QD's reference system (x, y, z) with respect to the lab system (X, Y, Z) is determined by three angles Ω, Ψ, and ω. **(b)** Schematic of the defocused wide-field fluorescence imaging microscope. **(c)** Sum image of a series of 50 frames (512×512 pixels) of the single QDs emission at a defocusing value of -0.82 μm with a magnification of $M = 330$. The exposure time of each frame is 100 ms. **(d)** The inset in (c) is the defocused images of single QDs on glass coverslip. **(e)** Defocused patterns of single QDs in ITO film which are magnified views of the red boxed regions in (a). **(f)** The corresponding calculated theoretical fits. **(g)** Five typical defocused patterns of single QDs on glass coverslip. **(h)** The corresponding calculated theoretical fits.

imaging microscope is depicted in Fig. 2(b). Defocused imaging is obtained by moving the objective with a distance of 1.00 ± 0.25 μm towards the samples (defocusing value). Figures 2(c) and (d) show typical defocused images of QDs in ITO film and on glass coverslip, respectively. Several typical defocused patterns and the corresponding theoretical fits for single QDs in ITO film and on glass coverslip are shown in Figs. 2(e)–(h), respectively. For single QDs on glass coverslips, the defocused patterns are similar to that of the previous literatures [50, 51]. However, it can be found that defocused patterns of single QDs encased in ITO film are very different from that of glass coverslips, and many of them show a clear bilateral symmetry which is similar to the emitters with single linear dipole, such as single dye molecules [45–47].

The defocused images were analyzed with a home-built MatLab routine according to the multidimensional dipole model developed by Enderlein and co-workers [50]. The final intensity distribution of defocused images of the three perpendicular dipoles measured by an EMCCD camera is proportional to $P = kI_z + (1-k)\left(\frac{1+\mu}{2}I_y + \frac{1-\mu}{2}I_x\right)$, where I_x, I_y, and I_z are the emitting intensities of three dipoles with the unit emission strength, and the two parameters k and μ define the intensity ratios of the three dipoles, respectively. The value pairs with $k = 0$ and μ close to zero correspond to a circular degenerate dipole emitter, and the values with $k = 1$ correspond to a purely linear dipole emitter [50]. For the single QDs on glass coverslip in Fig. 2(h), the parameter values of (Ω, Ψ, ω, k, μ) from theoretical fits for the five QDs are: (16, 168, 31, 0.2, 0), (0, 118, 0, 0.14, 0), (2, 323, 0, 0, 0), (19, 50, 0, 0.08, 0), and (24, 200, 0, 0.2, 0), respectively. However, the parameter values of (Ω, Ψ, ω, k, μ) from theoretical fits for the five QDs in ITO film in Fig. 2(f) are: (80, 165, 203, 1, −1), (56, 113, 180, 1, −1), (77, 192, 73, 1, −1), (83, 233, 80, 1, −1), and (59, 88, 80, 1, −1), respectively. By comparing the fitting parameters of k and μ in the two cases, these QDs in ITO film ($k = 1$) show a distinct linear dipole behavior, while the single QDs on glass coverslip are close to circular degenerate dipole emitters. We have analyzed

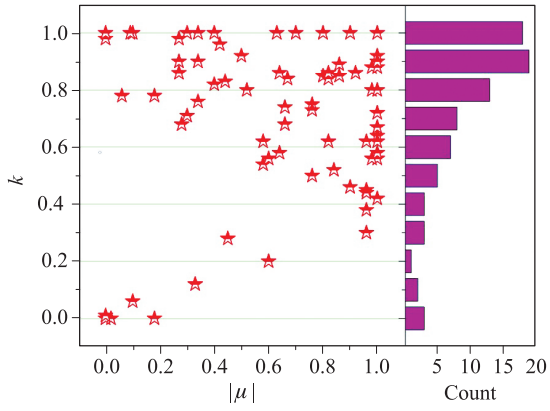

Fig. 3 Relation between the best-fit parameter values of k and $|\mu|$ for ~ 85 evaluated QDs in ITO films. The values of k close to 1 correspond to a linear dipole emitter.

the defocused images for ~ 85 single QDs in ITO film, and the absolute values of μ against the values of k are shown in Fig. 3. From the histogram of k in Fig. 3, we can find more than half of single QDs with $k \geq 0.7$, which indicates the z dipole (I_z) has much stronger emission strength than the others.

3.2 Polarization measurements for single QDs encased in ITO films

The linear dipole behavior of single QDs encased in ITO films has been shown visually by the defocused wide-field imaging. Here, we assess the polarization degrees by the method of polarization measurements. The polarization measurement of an emitter is normally performed in the far field by emission polarization analysis [23, 39]. Here, the emission polarization property of single QDs encased in ITO film is measured by single particle polarization microscopy as showed in Fig. 4(a). Polarization measurements are realized on single particles with a rotating broadband half-wave plate combined with a broadband polarizing beamsplitter cube. When a single QD is excited by a laser, the PL is collected by a high numerical aperture objective. The polarization dependence of emission for single QDs on glass coverslip is found to be significantly weak, and it is due to the fact that multiple, overlapping states emit simultaneously, decreasing the polarization degree in emission [33, 52].

The typical PL trajectories plotted as a function of the half-wave plate angle are shown in Fig. 4(b). The trajectories were recorded with an integration time of 10 ms, and the rotational speed of the half-wave plate was set to 6° s^{-1}. When the half-wave plate rotates from 0° to 180°, the linear polarized photons rotate from 0° to 360° and thus there are two modulation cycles for single QD's emission. The polarization degree (p) is defined by $p = (I_{\max} - I_{\min})/(I_{\max} + I_{\min})$, where $I_{\max}$ and $I_{\min}$ correspond to the maximum and minimum detector counts in an emission modulation cycle. $I_{\max}$ and $I_{\min}$ can be obtained by fitting to the function, $I(\theta_{\lambda/2}) = (I_{\max} - I_{\min})\cos^2(\theta_{\lambda/2}) + I_{\min}$ [blue lines in Fig. 4(b)], where $\theta_{\lambda/2}$ is the angle of the half-wave plate [23, 39]. The resulting fits for the trajectories in Fig. 4(b) yield $p = 0.41$ (upper part) and $p = 0.62$ (lower part) respectively. The phase difference between them is about 45° with respect to the half-wave plate angle. Noting that fluorescence blinking can be observed in the trajectories, which is attributed to the photoinduced charging of QDs by electron transfer to trap states [5, 20, 53]. The average background has been subtracted from the trajectories before fitting. However, the fitting errors due to fluorescence blinking and the inhomogeneity of background lead to the experimental error of $\sim 5\%$ in the assessment of the polarization degree. Figure 4(c) shows the histogram of p for ~ 158 QDs in ITO films. By fitting the histogram with a Gaussian distribution, the average value with standard deviation of p is 0.45 ± 0.17.

Here, we do not show the results of polarization measurement for single QDs on glass coverslip, because it is very difficult to extract the polarization information from the PL traces due to the strong blinking as well as the long dark states in this case [20]. However, we have estimated the polarization degree of single QDs by considering the aspect ratios of QDs according to the theory in Refs. [39, 52]. The calculated polarization degree as a function of aspect ratio is shown in Fig. S1(b) in the Supporting Information, and the polarization degree is smaller than 0.15 for the various aspect ratios. Therefore, these results reveal that ITO nanoparticles should be accountable for the linear dipole behaviors of single QDs.

3.3 The possible mechanism for the linear dipole behavior of single QDs

Here, we give a possible mechanism for the linear dipole behavior of single QDs according to the previous reports on the CdSe/OPV system [40, 41]. Here, the ITO has a higher Fermi level than that of the QDs, therefore the electrons in ITO will be transferred to QDs due to the Fermi level equilibration [5, 20]. Quantitative electrostatic force microscopy measurements have also revealed that there are 2–3 electrons on single QD surface when QDs are in contact with ITO [17]. By atomistic empirical pseudopotential calculations, Wang has demonstrated that the electric field set up by a classic point charge located near the surface of a QD can substantially alter the distribution of the photogenerated electron and hole wave functions [54]. For example, when a negative external charge is near the surface of CdSe QD, its Coulomb potential could be strong enough to pull the hole from the electron and results in a reduction of the overlap between electron and hole wave functions. By computing the first order Stark corrections to the $1S_e$ and $1S_{3/2,M}$ electron/hole wavefunctions [41], Early *et al.* suggested that the Stark distortion of the quantum dot electron/hole wavefunctions

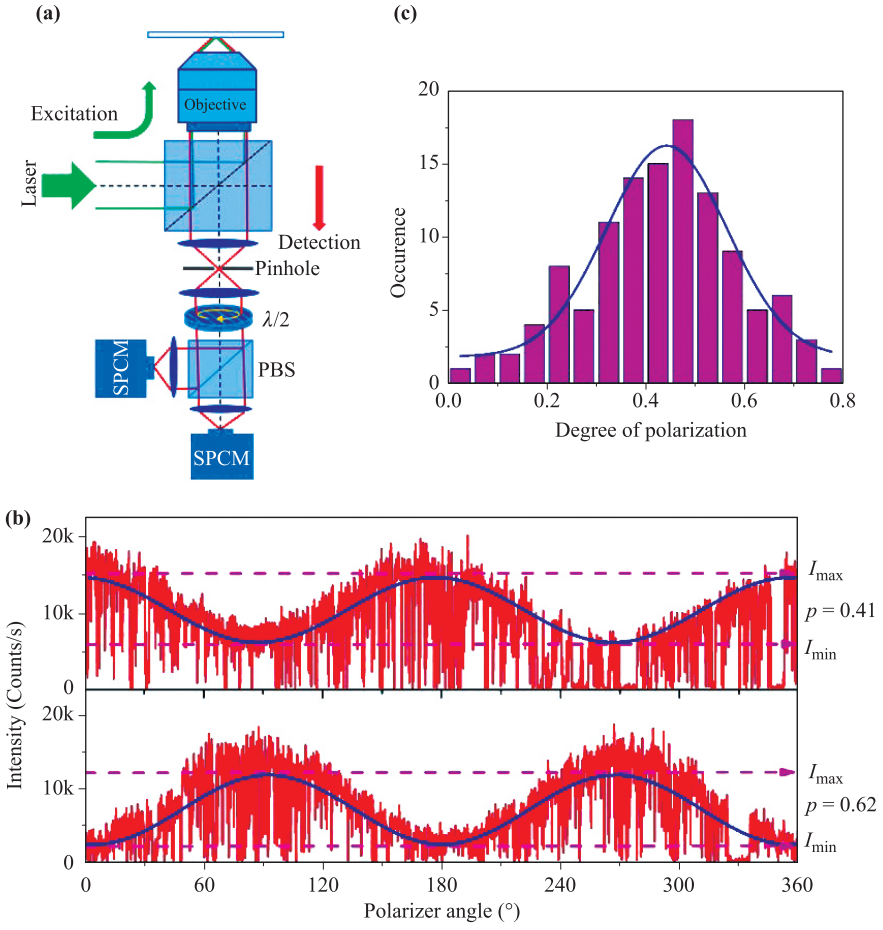

Fig. 4 Schematic of experimental setup, and results of polarization measurement. **(a)** Scheme of the setup for single particle polarization measurement. A picosecond pulsed diode laser of $\lambda = 635$ nm is used to excite single QDs. The fluorescence is collected by an objective and is directed to a combination of a broadband half-wave plate and a polarizing beamsplitter cube for the analysis of the degree of polarization. **(b)** Experimental polarization measurement trajectories for two typical single QDs in ITO film, and the fluorescence signal from one of single photon detectors (red line) is plotted as a function of the half-wave plate angle. The trajectories are fitted by $I(\theta_{\lambda/2}) = (I_{max} - I_{min})\cos^2(\theta_{\lambda/2}) + I_{min}$ function to derive the degree of polarization (p). The phase offset of the two single QDs is real, showing no experimental polarization bias. **(c)** Histogram of the polarization degrees for ~ 158 QDs, with an average polarization degree of 0.45 ± 0.17.

results in the linear polarization property of single QDs. Based on the discussion, we attribute the linear dipole behavior of single QDs to the surface electrons induced the Stark distortion of the QD electron/hole wavefunctions.

4 Conclusions

In the paper, we have demonstrated the linear dipole behavior of single QDs in ITO films using both defocused wide-field fluorescence imaging and single particle polarization measurement techniques. The defocused wide-field imaging has visualized the linear dipole emission of single QDs encased in ITO films. The average polarization degree has been determined to be ~ 0.45 by the single particle polarization measurement. The linear dipole behavior of single QDs is attributed to the surface electrons induced the Stark distortion of the QD electron/hole wavefunctions. The polarization degrees show a significant difference from dot to dot due to the heterogeneous interactions between the surface electrons and the photogenerated electron/hole within the QDs. The metal oxide nanoparticles induced linear dipole behavior has significant implications in photon absorption and energy transfer, relevant to QD-based photovoltaics and optoelectronics.

Electronic supplementary material Supplementary material is available in the online version of this article at https://doi.org/10.1007/s11467-018-0874-z and is accessible for authorized users.

Acknowledgements We gratefully acknowledge financial support from the National Key R&D Program of China (No. 2017YFA0304203), the National Natural Science Foundation of China (Grant Nos. 61527824, 61675119, U1510133, 11434007, 11504216, and 61605104), PCSIRT (No. IRT_17R70). Y. Peng was supported by the National Natural Science Foundation

of China (No. 11404189). H. Xie was supported by the National Natural Science Foundation of China (No. 11504260).

References

1. M. R. Kim and D. L. Ma, Quantum-dot-based solar cells: Recent advances, strategies, and challenges, *J. Phys. Chem. Lett.* 6(1), 85 (2015)
2. J. Kwak, J. Lim, M. Park, S. Lee, K. Char, and C. Lee, High-power genuine ultraviolet light-emitting diodes based on colloidal nanocrystal quantum dots, *Nano Lett.* 15(6), 3793 (2015)
3. C. H. M. Chuang, P. R. Brown, V. Bulovic, and M. G. Bawendi, Improved performance and stability in quantum dot solar cells through band alignment engineering, *Nat. Mater.* 13(8), 796 (2014)
4. G. C. Shan, Z. Q. Yin, C. H. Shek, and W. Huang, Single photon sources with single semiconductor quantum dots, *Front. Phys.* 9(2), 170 (2014)
5. S. Y. Jin, N. H. Song, and T. Q. Lian, Suppressed blinking dynamics of single QDs on ITO, *ACS Nano* 4(3), 1545 (2010)
6. N. H. Song, H. M. Zhu, Z. Liu, Z. Q. Huang, D. Wu, and T. Q. Lian, Unraveling the exciton quenching mechanism of quantum dots on antimony-doped SnO_2 films by transient absorption and single dot fluorescence spectroscopy, *ACS Nano* 7(2), 1599 (2013)
7. H. Cho, J. Kwak, J. Lim, M. Park, D. Lee, W. K. Bae, Y. S. Kim, K. Char, S. Lee, and C. Lee, Soft contact transplanted nanocrystal quantum dots for light-emitting diodes: Effect of surface energy on device performance, *ACS Appl. Mater. Interfaces* 7(20), 10828 (2015)
8. G. Luo, Z. Z. Zhang, H. O. Li, X. X. Song, G. W. Deng, G. Cao, M. Xiao, and G. P. Guo, Quantum dot behavior in transition metal dichalcogenides nanostructures, *Front. Phys.* 12(4), 128502 (2017)
9. Q. B. Zeng, S. Chen, L. You, and R. Lu, Transport through a quantum dot coupled to two majorana bound states, *Front. Phys.* 12(4), 127302 (2017)
10. S. Y. Jin and T. Q. Lian, Electron transfer dynamics from single CdSe/ZnS quantum dots to TiO_2 nanoparticles, *Nano Lett.* 9(6), 2448 (2009)
11. J. M. Luther, M. Law, M. C. Beard, Q. Song, M. O. Reese, R. J. Ellingson, and A. J. Nozik, Schottky solar cells based on colloidal nanocrystal films, *Nano Lett.* 8(10), 3488 (2008)
12. W. Ma, S. L. Swisher, T. Ewers, J. Engel, V. E. Ferry, H. A. Atwater, and A. P. Alivisatos, Photovoltaic performance of ultrasmall PbSe quantum dots, *ACS Nano* 5(10), 8140 (2011)
13. J. Tang, H. Liu, D. Zhitomirsky, S. Hoogland, X. Wang, M. Furukawa, L. Levina, and E. H. Sargent, Quantum junction solar cells, *Nano Lett.* 12(9), 4889 (2012)
14. Z. Ning, Y. Ren, S. Hoogland, O. Voznyy, L. Levina, P. Stadler, X. Lan, D. Zhitomirsky, and E. H. Sargent, All-inorganic colloidal quantum dot photovoltaics employing solution-phase halide passivation, *Adv. Mater.* 24(47), 6295 (2012)
15. A. Issac, S. Y. Jin, and T. Q. Lian, Intermittent electron transfer activity from single CdSe/ZnS quantum dots, *J. Am. Chem. Soc.* 130(34), 11280 (2008)
16. P. P. Jha and P. Guyot-Sionnest, Trion decay in colloidal quantum dots, *ACS Nano* 3(4), 1011 (2009)
17. S. E. Yalcin, B. Q. Yang, J. A. Labastide, and M. D. Barnes, Electrostatic force microscopy and spectral studies of electron attachment to single quantum dots on indium tin oxide substrates, *J. Phys. Chem. C* 116(29), 15847 (2012)
18. Y. Nagao, H. Fujiwara, and K. Sasaki, Analysis of trap-state dynamics of single CdSe/ZnS quantum dots on a TiO_2 substrate with different Nb concentrations, *J. Phys. Chem. C* 118(35), 20571 (2014)
19. H. W. Cheng, C. T. Yuan, J. S. Wang, T. N. Lin, J. L. Shen, Y. J. Hung, J. Tang, and F. G. Tseng, Modification of photon emission statistics from single colloidal CdSe quantum dots by conductive materials, *J. Phys. Chem. C* 118(31), 18126 (2014)
20. B. Li, G. Zhang, Z. Wang, Z. Li, R. Chen, C. Qin, Y. Gao, L. Xiao, and S. Jia, Suppressing the fluorescence blinking of single quantum dots encased in N-type semiconductor nanoparticles, *Sci. Rep.* 6(1), 32662 (2016)
21. Z. J. Li, G. F. Zhang, B. Li, R. Y. Chen, C. B. Qin, Y. Gao, L. T. Xiao, and S. T. Jia, Enhanced biexciton emission from single quantum dots encased in N-type semiconductor nanoparticles, *Appl. Phys. Lett.* 111(15), 153106 (2017)
22. P. P. Jha and P. Guyot-Sionnest, Electrochemical switching of the photoluminescence of single quantum dots, *J. Phys. Chem. C* 114(49), 21138 (2010)
23. C. Lethiec, J. Laverdant, H. Vallon, C. Javaux, B. Dubertret, J. M. Frigerio, C. Schwob, L. Coolen, and A. Maitre, Measurement of three-dimensional dipole orientation of a single fluorescent nanoemitter by emission polarization analysis, *Phys. Rev. X* 4(2), 021037 (2014)
24. A. G. Silva, C. A. Parra-Murillo, P. T. Valentim, J. S. Morais, F. Plentz, P. S. Guimaraes, H. Vinck-Posada, B. A. Rodriguez, M. S. Skolnick, A. Tahraoui, and M. Hopkinson, Quantum dot dipole orientation and excitation efficiency of micropillar modes, *Opt. Express* 16(23), 19201 (2008)
25. X. Brokmann, L. Coolen, J. P. Hermier, and M. Dahan, Emission properties of single CdSe/ZnS quantum dots close to a dielectric interface, *Chem. Phys.* 318(1–2), 91 (2005)
26. Q. A. Li, X. J. Chen, Y. Xu, S. Lan, H. Y. Liu, Q. F. Dai, and L. J. Wu, Photoluminescence properties of the CdSe quantum dots accompanied with rotation of the defocused wide-field fluorescence images, *J. Phys. Chem. C* 114(32), 13427 (2010)

27. W. D. Sheng, M. Korkusinski, A. D. Guclu, M. Zielinski, P. Potasz, E. S. Kadantsev, O. Voznyy, and P. Hawrylak, Electronic and optical properties of semiconductor and graphene quantum dots, *Front. Phys.* 7(3), 328 (2012)
28. J. J. Macklin, J. K. Trautman, T. D. Harris, and L. E. Brus, Imaging and time-resolved spectroscopy of single molecules at an interface, *Science* 272(5259), 255 (1996)
29. P. Dedecker, B. Muls, A. Deres, H. Uji-i, J. Hotta, M. Sliwa, J. P. Soumillion, K. Müllen, J. Enderlein, and J. Hofkens, Defocused wide-field imaging unravels structural and temporal heterogeneity in complex systems, *Adv. Mater.* 21(10–11), 1079 (2009)
30. G. F. Zhang, L. T. Xiao, F. Zhang, X. B. Wang, and S. T. Jia, Single molecules reorientation reveals the dynamics of polymer glasses surface, *Phys. Chem. Chem. Phys.* 12(10), 2308 (2010)
31. T. Ha, T. Enderle, S. Chemla, R. Selvin, and S. Weiss, Single molecule dynamics studied by polarization modulation, *Phys. Rev. Lett.* 77(19), 3979 (1996)
32. R. Y. Chen, G. F. Zhang, C. B. Qin, Y. Gao, L. T. Xiao, and S. T. Jia, Modification of single molecule fluorescence using external fields, *Front. Phys.* 12(5), 128101 (2017)
33. A. L. Efros, Luminescence polarization of CdSe microcrystals, *Phys. Rev. B* 46(12), 7448 (1992)
34. A. L. Efros and A. V. Rodina, Band-edge absorption and luminescence of nonspherical nanometer-size crystals, *Phys. Rev. B* 47(15), 10005 (1993)
35. J. T. Hu, L. S. Li, W. D. Yang, L. Manna, L. W. Wang, and A. P. Alivisatos, Linearly polarized emission from colloidal semiconductor quantum rods, *Science* 292(5524), 2060 (2001)
36. H. Htoon, M. Furis, S. A. Crooker, S. Jeong, and V. I. Klimov, Linearly polarized 'fine structure' of the bright exciton state in individual CdSe nanocrystal quantum dots, *Phys. Rev. B* 77(3), 035328 (2008)
37. D. Montiel and H. Yang, Observation of correlated emission intensity and polarization fluctuations in single CdSe/ZnS quantum dots, *J. Phys. Chem. A* 112(39), 9352 (2008)
38. C. Lethiec, F. Pisanello, L. Carbone, A. Bramati, L. Coolen, and A. Maitre, Polarimetry-based analysis of dipolar transitions of single colloidal CdSe/CdS dot-in-rods, *New J. Phys.* 16(9), 093014 (2014)
39. S. Vezzoli, M. Manceau, G. Lemenager, Q. Glorieux, E. Giacobino, L. Carbone, M. De Vittorio, and A. Bramati, Exciton fine structure of CdSe/CdS nanocrystals determined by polarization microscopy at room temperature, *ACS Nano* 9(8), 7992 (2015)
40. K. T. Early, K. D. McCarthy, M. Y. Odoi, P. K. Sudeep, T. Emrick, and M. D. Barnes, Linear dipole behavior in single CdSe-oligo(phenylene vinylene) nanostructures, *ACS Nano* 3(2), 453 (2009)
41. K. T. Early, P. K. Sudeep, T. Emrick, and M. D. Barnes, Polarization-driven stark shifts in quantum dot luminescence from single CdSe/oligo-PPV nanoparticles, *Nano Lett.* 10(5), 1754 (2010)
42. N. I. Hammer, K. T. Early, K. Sill, M. Y. Odoi, T. Emrick, and M. D. Barnes, Coverage-mediated suppression of blinking in solid state quantum dot conjugated organic composite nanostructures, *J. Phys. Chem. B* 110(29), 14167 (2006)
43. M. Y. Odoi, K. T. Early, R. Tangirala, P. K. Sudeep, T. Emrick, and M. D. Barnes, Probing multiexcitonic emission in single CdSe-oligo(phenylenevinylene) composite nanostructures, *J. Phys. Chem. C* 113(31), 13462 (2009)
44. S. Rühle, Tabulated values of the shockley-queisser limit for single junction solar cells, *Sol. Energy* 130, 139 (2016)
45. A. Deres, G. A. Floudas, K. Müllen, M. Van der Auweraer, F. De Schryver, J. Enderlein, H. Uji-i, and J. Hofkens, The origin of heterogeneity of polymer dynamics near the glass temperature as probed by defocused imaging, *Macromolecules* 44(24), 9703 (2011)
46. M. Böhmer and J. Enderlein, Orientation imaging of single molecules by wide-field epifluorescence microscopy, *J. Opt. Soc. Am. B* 20(3), 554 (2003)
47. D. Patra, I. Gregor, and J. Enderlein, Image analysis of defocused single-molecule images for three-dimensional molecule orientation studies, *J. Phys. Chem. A* 108(33), 6836 (2004)
48. T. Ihara, R. Sato, T. Teranishi, and Y. Kanemitsu, Delocalized and localized charged excitons in single CdSe/CdS dot-in-rods revealed by polarized photoluminescence blinking, *Phys. Rev. B* 90(3), 035309 (2014)
49. F. Hu, B. Lv, C. Yin, C. Zhang, X. Wang, B. Lounis, and M. Xiao, Carrier multiplication in a single semiconductor nanocrystal, *Phys. Rev. Lett.* 116(10), 106404 (2016)
50. D. Patra, I. Gregor, J. Enderlein, and M. Sauer, Defocused imaging of quantum-dot angular distribution of radiation, *Appl. Phys. Lett.* 87(10), 101103 (2005)
51. R. Schuster, M. Barth, A. Gruber, and F. Cichos, Defocused wide field fluorescence imaging of single CdSe/ZnS quantum dots, *Chem. Phys. Lett.* 413(4–6), 280 (2005)
52. A. L. Efros, M. Rosen, M. Kuno, M. Nirmal, D. J. Norris, and M. Bawendi, Band-edge exciton in quantum dots of semiconductors with a degenerate valence band: Dark and bright exciton states, *Phys. Rev. B* 54(7), 4843 (1996)
53. C. Galland, Y. Ghosh, A. Steinbrück, M. Sykora, J. A. Hollingsworth, V. I. Klimov, and H. Htoon, Two types of luminescence blinking revealed by spectroelectrochemistry of single quantum dots, *Nature* 479(7372), 203 (2011)
54. L. W. Wang, Calculating the influence of external charges on the photoluminescence of a CdSe quantum dot, *J. Phys. Chem. B* 105(12), 2360 (2001)